INSTITUT DE FRANCE
Académie des sciences

Comptes Rendus

Chimie

Chingis Daulbayev, Fail Sultanov, Maiya Aldasheva, Aliya Abdybekova, Baglan Bakbolat, Mohammad Shams, Aruzhan Chekiyeva and Zulkhair Mansurov

Nanofibrous biologically soluble scaffolds as an effective drug delivery system

Volume 24, issue 1 (2021), p. 1-9

Published online: 23 February 2021

https://doi.org/10.5802/crchim.58

Les Comptes Rendus. Chimie *sont membres du*
Centre Mersenne pour l'édition scientifique ouverte
www.centre-mersenne.org
e-ISSN : 1878-1543

Comptes Rendus
Chimie
2021, 24, nº 1, p. 1-9
https://doi.org/10.5802/crchim.58

Full paper / *Article*

Nanofibrous biologically soluble scaffolds as an effective drug delivery system

Chingis Daulbayev [a, b], Fail Sultanov [*, a, b], Maiya Aldasheva [c], Aliya Abdybekova [d], Baglan Bakbolat [a, b], Mohammad Shams [a, b], Aruzhan Chekiyeva [e] and Zulkhair Mansurov [a, b]

[a] al-Farabi Kazakh National University, 050038, Almaty, Kazakhstan

[b] Institute of Combustion Problems, 050012, Almaty, Kazakhstan

[c] S.D. Asfendiyarov Kazakh National Medical University, 050012, Almaty, Kazakhstan

[d] Kazakh Medical University of Continuing Education, 050040, Almaty, Kazakhstan

[e] K.I. Satbayev Kazakh National Research Technical University, 050013, Almaty, Kazakhstan

E-mails: chingis.daulbayev@yandex.ru (C. Daulbayev), fail_bk@bk.ru (F. Sultanov), maya_aldasheva@mail.ru (M. Aldasheva), aliya_abdybekova@mail.ru (A. Abdybekova), baglan.bakbolat@mail.ru (B. Bakbolat), shams.m.iau@gmail.com (M. Shams), aruqkz@gmail.com (A. Chekiyeva), zmansurov@kaznu.kz (Z. Mansurov)

Abstract. In this article, the synthesis of biocompatible fibrous scaffolds with antimicrobial properties based on polycaprolactone/hydroxyapatite/amoxicillin and study of their surface morphology, antimicrobial effect, and drug release are discussed. Hydroxyapatite (1–2 μm, 97%) synthesized from biologically waste material (eggshell) was added to the composite scaffolds as a bone-replacement material. The scaffolds' antimicrobial properties were evaluated against *S. aureus* and *E. faecalis*. The scaffolds possessed a sustained drug release from the scaffolds amounted to about 94% of the antibiotic's total weight over a 4-week observation period. Agar diffusion confirmed the antimicrobial properties of the scaffolds against specific bacteria.

Keywords. Electrospinning, Hydroxyapatite, Biologically soluble scaffolds, Fibers, Drugs.

Manuscript received 13th July 2020, revised 9th November 2020 and 13th November 2020, accepted 17th November 2020.

1. Introduction

The presence of various microorganisms in the oral cavity can develop caries and other accompanying complications [1–3]. Without specific treatment, caries of enamel affects the underlying tissues of teeth, leading to infection of the pulp and death with the subsequent development of apical periodontitis [4].

The modern apical periodontitis treatment methods based on endodontic therapy of the root help remove the infected pulp and fill the canals with synthetic materials to eliminate the infection and prevent the subsequent microbial invasion [5–7]. The main drawback of endodontic therapy methods is

* Corresponding author.

that they cannot fully disinfect the root canals because of their complex anatomy [8]. The complex anatomy of the root canal systems prevents the complete contact of chemical–mechanical preparations and antimicrobial agents. In this regard, the use of biologically soluble scaffolds with the optimal content of antimicrobial reagents and the possibility of their prolonged release is one of the ways to increase the effectiveness of the treatment [9–14].

In its turn, the use of biodegradable polymer scaffolds with the addition of calcium hydroxyapatite (HAP) is a promising and developing area of regenerative endodontic therapy [15–18]. HAP promotes hard bone tissue formation, which is extremely important for endodontic therapy of apical periodontitis with progressive bone resorption around the tooth root [19]. Therefore, it is one of the recommended materials in the treatment of dental tissue defects [20–23]. At present, the use of HAP mainly focuses on formation of pastes, powders, or granules, limiting its widespread application [24].

The use of electrospun biologically soluble scaffolds with antimicrobial agents and HAP in endodontic therapy can enhance the effectiveness of disinfection of root systems and targeted delivery of active substances to the local points of infection. The advantage of this method lies in creating a base substrate for cell proliferation with the ability to simultaneously control the diameter of the forming polymer fibers and the number of active substances in the structure of the resulting scaffold. Numerous research [25–29] demonstrated the high efficiency of biological polymer scaffolds obtained by electrospinning in regenerative endodontic therapy. The possibility of using various biomaterials, polymers and drugs, in the form of both a powder and a solution, allows using the electrospinning method to create composite structures on a nanometer scale.

Considering the above mentioned facts, the use of biologically soluble scaffolds containing HAP and antimicrobial reagents is one of the possible solutions to increase the endodontic treatment effectiveness. Of great importance is the possibility of selecting optimal types of antibiotics, which are highly effective in treating apical periodontitis. Therefore, amoxicillin (AMX), a broad-spectrum antibiotic of the penicillin group and the most effective antibiotic for apical periodontitis treatment was chosen as an additive to the forming scaffolds. Moreover, it refers to the Access group according to the AWaRe Classification antibiotics (WHO, 2017) [30]. This group consists of antibiotics with a low resistance potential and a broad spectrum of activity to commonly encountered pathogens, including the leading representatives of aerobic and anaerobic microflora in the root canals of teeth.

In this research, the composite biologically soluble polymer scaffolds with the addition of HAP and an antibiotic (AMX) were obtained by electrospinning, which is a simple and effective method for producing composite nanoscale fibers, and the kinetics of local drug delivery in endodontic treatment was investigated. Scanning electron microscopy (SEM) and X-ray analysis were used to study the surface morphology and chemical composition of the obtained scaffolds; the drug release kinetics was analyzed by high-performance liquid chromatography (HPLC). It is expected that biologically soluble scaffolds with the addition of HAP and AMX will inhibit the growth of pathogenic microorganisms and favor the prolonged release of the antibiotic, while the presence of HAP will promote the formation of hard bone tissues.

2. Materials and methods

2.1. *HAP synthesis*

The initial materials for crystalline HAP preparation are orthophosphoric acid (H_3PO_4, 85%, Sigma Aldrich) and eggshell waste, which was used as a calcium-containing component. First, a weighted amount of eggshells (4 g) was annealed to 950 °C for two hours with the evaporation of volatile compounds and the formation of calcium oxide (CaO). The resulting CaO powder (2 g) was mixed with an aqueous solution of phosphoric acid (6%, 40 mL) under constant stirring for 1 h, followed by its ultrasonic treatment in an ice bath at a frequency of 32 kHz for 1 h until complete homogenization. Finally, the mixture was dried in vacuum at a temperature of 110 °C for 24 h.

2.2. *Electrospinning of scaffolds based on PCL/HAP/AMX*

Polycaprolactone (PCL, average M.W. 1,300,000, Sigma Aldrich) and dimethylformamide (99.9%, Sigma Aldrich) were used to prepare the polymer

solution for electrospinning. First, PCL (2 g) was dissolved in dimethylformamide (10 mL) under magnetic stirring for 20 min (120 rpm) at 50 °C. Then, HAP powder (0.5 g) and AMX (0.6 mL) were added to the polymer solution. The polymer mixture with the added components was stirred until its complete homogenization, then a 10 mL medical syringe was filled with the solution. The process of electrospinning of polymer fibers was performed at room temperature, the value of voltage was 15 kV, and the precursor feed rate was 0.5 mL/h.

2.3. *Evaluation of the microbiological effectiveness of scaffolds based on PCL/HAP/AMX*

The antimicrobial properties of bioscaffolds based on PCL/HAP/AMX were studied on *S. aureus* and *E. faecalis*, which are the prominent representatives of aerobic and facultative anaerobic microflora of the root canals. Three types of bioscaffolds with different PCL, HAP, and AMX contents (PCL with 7 wt% of HAP and 5 wt% of AMX; PCL with 7 wt% of HAP; and pure PCL) were prepared. Antibiotic-free samples served as negative control. The obtained samples (15×15 mm^2) were placed in well plates and disinfected by adding 2 mL of 70% ethanol with an exposure time of 30 min, then they were washed twice with 2 mL of 0.9% isotonic solution. The bacterial suspension of the investigated germs was prepared from several daily colonies grown on nutrient agar in correspondence to the 0.5 McFarland turbidity standard. To inoculate the nutrient medium, a sterile cotton swab was immersed into the suspension with removing the inoculum excess and seeded onto the surface of Mueller–Hinton agar with dashed movements by rotating the Petri dish. Then, six Petri dishes were used for the study: the reference strain of *S. aureus* 209P was inoculated on the first three of them, while the bacterial culture of *E. faecalis* (an archival strain of S.D. Asfendiyarov Kazakh National Medical University) was inoculated on the remaining three dishes. Within 15 min, three samples (one from each type of bioscaffolds) were placed on the surface of the dishes inoculated with *S. aureus* 209P; the remaining three samples were placed on the dishes inoculated with *E. faecalis* and incubated in a thermostat at 37 °C for 24 h. The antibacterial properties were recorded after 24 and 72 h by measuring the bacterial growth inhibition zone (mm) around the scaffold sample.

2.4. *Scaffolds based on PCL/HAP/AMX drug release measurements*

The scaffolds obtained with the addition of HAP and AMX were loaded into flasks with 10 mL of phosphate buffer solution and placed in an horizontal incubator, which was rotated with a rate of 40 rpm at the temperature of 33 °C. The amount of the released drug was determined using a Varian Cary 300 spectrophotometer under UV-irradiation with a wavelength of 272 nm.

2.5. *Characterization of the obtained samples*

The morphology of biologically soluble scaffolds was analyzed using scanning electron microscope QUANTA 3D 200i with an accelerating voltage of 15 kV. XRD analysis was carried out on an X-ray diffractometer of the type Drone-4 with the diffraction rotation angles ranging from −100° to 168°. The minimum step of moving the detecting unit is 0.001. The admissible deviation of the detecting unit from the specified angle of rotation is ±0.015.

3. Results and discussion

3.1. *Synthesis and study of HAP*

Overall, the crystalline HAP powder was synthesized by the chemical reaction of CaO with H_3PO_4. The eggshell waste mainly consists of calcium carbonate ($CaCO_3$), which decomposes to CaO and CO_2 during its thermal treatment at 850–1000 °C.

$$CaCO_3 \rightarrow CaO + CO_2 (T = 850\text{–}1000\ ^\circ C) \quad (1)$$

During the thermal treatment, organic components of eggshells evaporate, and the resulting residue mainly contains CaO with a small impurity content (≤1%). After thermal treatment, the formed CaO was put into a glass beaker and mixed with a 6% aqueous solution of H_3PO_4 under vigorous stirring. As a result, calcium hydroxide is formed (2).

$$CaO + H_2O \rightarrow Ca(OH)_2 + Q \quad (2)$$

Based on experimental results, it was found that for the complete reaction (3), it is necessary to stir the suspension for one hour after adding the acid. The amount of acid required for the complete reaction to obtain HAP was calculated according to (3).

$$10Ca(OH)_2 + 6H_3PO_4 \rightarrow Ca_{10}(PO_4)_6(OH)_2 + 18H_2O \quad (3)$$

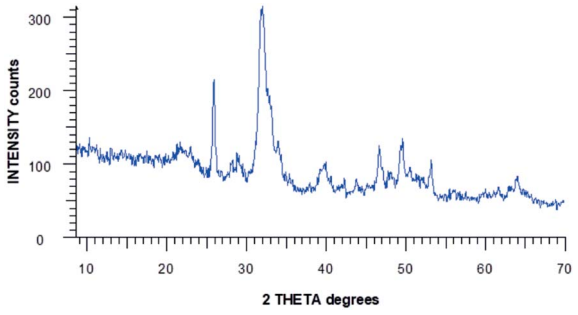

Figure 1. X-ray pattern of synthesized HAP.

The process of synthesis of HAP was controlled by maintaining the pH of the mixture in the range from 6 to 8 throughout the reaction in order to obtain HAP with the required Ca/P ratio close to 1.67, which corresponds to the formation of stoichiometric HAP with good crystallinity and purity [31,32].

The crystal structure of the obtained HAP was investigated by X-ray phase analysis (Figure 1). All diffraction peaks correspond to the hexagonal structure of synthesized HAP and are in agreement with the JCPDS (Joint Committee for Powder Diffraction Standards) data # 96-900-2219. According to the resulting X-ray diffraction pattern, the purity of the obtained HAP powder is more than 97%, while no characteristic impurity peaks, such as calcium hydroxide or calcium phosphates, were observed.

SEM images of the obtained HAP samples demonstrate the presence of crystals with submicron and nanoscale inclusions. The microstructure of samples is presented in the form of angular and bulk crystals, with an average size of 1–2 μm with a rough layered structure and a developed surface morphology (Figure 2).

The synthesized HAP was further subjected to a post-thermal treatment at a temperature of 1100 °C in an air medium for three hours to increase its crystallinity and enhance its mechanical properties. The X-ray diffraction patterns of the HAP before post-thermal treatment (line 1) and after it (line 2) are presented in Figure 3. The main diffraction peaks corresponding to HAP are shifted toward smaller angles, and the interplanar spacing decreases, indicating a high degree of crystallinity of post-thermal treated HAP (Figure 3, line 2). Simultaneously, the broad peaks observed in the X-ray pattern of HAP without post-thermal treatment (Figure 3, line 1) indicate the heterogeneity of the structure and the presence of defects. The obtained experimental results indicate that during an increase in post-thermal temperature to 1100 °C, the crystal lattice parameters (a = 9.84218, $b = 2a$, c = 9.473) of the synthesized HAP are in correspondence with those of biocompatible HAP used as a biomaterial [33]. These results are confirmed by other studies [34], in which it was found that the density, bending strength, and Knoop hardness of HAP, thermally treated in air medium for four hours, increase with higher sintering temperatures, reaching a maximum at 1150 °C.

3.2. *Electrospinning of PCL/HAP/AMX based scaffolds*

PCL was chosen as a polymer to produce biologically soluble scaffolds with HAP and AMX by the electrospinning method since this polymer is biodegradable, biocompatible, non-immunogenic, non-carcinogenic, and non-toxic, which allow obtaining composite scaffolds that are widely used in tissue engineering [35]. Moreover, the chemical and biological properties of PCL, such as biological compatibility and mechanical strength, make it possible to use it for replacement of hard tissues in the body, in which healing also takes an extended period. Solutions for electrospinning were prepared with different ratios of components to study the effect of their concentration on the final properties of the scaffolds. The experiments showed that an increase in polymer concentration of the solution leads to the formation of fibers with a large diameter, which can be explained by the dependence of the diameter of forming fibers on the viscosity of the electrospinning solution (Supplementary information) [26]. The formation of PCL/HAP/AMX scaffolds was conducted via vertical arrangement of the syringe pump. It should be noted that under the influence of gravity in the horizontal position of the syringe pump, a precipitate is formed in the syringe. In turn, formation of a precipitate reduces the viscosity of the solution at the exit of the needle, affecting the diameter of polymer fiber. The influence of the solution feed rate, which varied from 1.5 to 3 mL/h, on the diameter of nanoscale fibers is related to the mechanisms of formation of a Taylor cone. At high solution feed rates, the Taylor cone does not have time to be formed, leading to formation of unstable

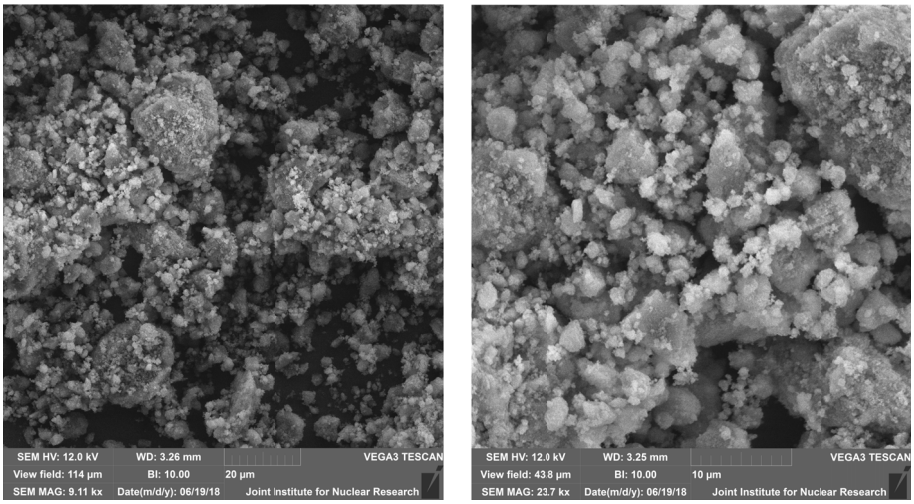

Figure 2. SEM images of synthesized HAP.

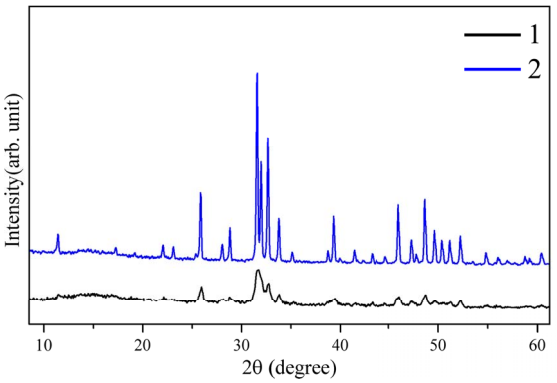

Figure 3. X-ray diffraction patterns of HAP: (1) HAP particles without post-thermal treatment; (2) HAP particles with post-thermal treatment at a temperature of 1100 °C for three hours.

nanoscale fibers. Figure 4 presents SEM images of the surface morphology of scaffolds based on PCL fibers with additions of HAP and AMX.

As shown in Figure 4, filamentous polymer fibers with agglomerates of HAP particles with an average diameter of polymer fibers from 100 nm to 200 nm are formed in the composite scaffold structure. Although the particles were obtained with an average size of 1–2 μm as a result of the synthesis of HAP powder, the size of the added HAP particles was found to be much smaller after electrospinning. This can be explained by the behavior of HAP particles during the stretching of polymer fibers under high voltage. The studies show that electrical exposure leads to the destruction of HAP particles. The presumable reason for this destruction is the action of an electric field, which is concentrated inside a solid dielectric, leading to a decrease in the size of HAP particles. This indicates the fact that high voltage promotes the stable formation of polymer fibers and causes the destruction of HAP particles.

Figure 5 presents the EDX analysis data demonstrating the elemental composition of the synthesized scaffold in the selected region.

Based on the results of EDX analysis, it can be concluded that the sample contains four elements: O (approximately 44.2 wt%), Ca (approximately 33.5 wt%), P (approximately 20.04 wt%), and C (approximately 6.5 wt%). The Ca/P ratio in the resulting composite sample was stated as 1.67, while the value of this parameter for synthetic and chemically pure HAP ranges from 0.5 to 2.0 [36].

3.3. *Assessment of the microbiological effectiveness and drug release of the PCL/HAP/AMX based scaffolds*

As a result of the standard agar diffusion test, significant inhibition of the studied bacterial strains growth was revealed around the synthesized bioscaffold (PCL + 7 wt% HAP + 5 wt% AMX). In the

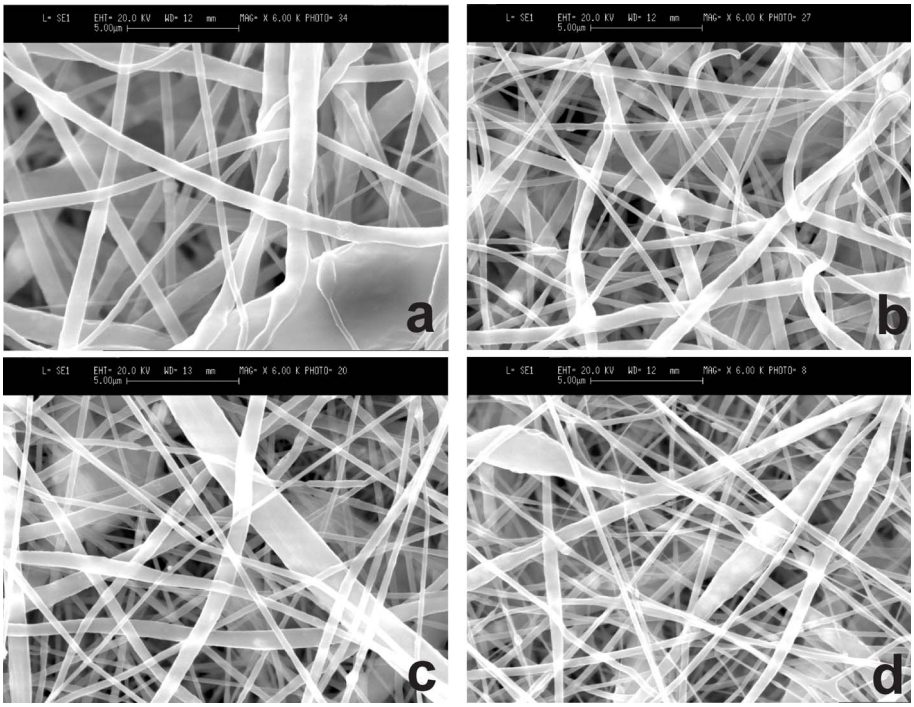

Figure 4. SEM images of the obtained bioscaffolds: (a) PCL based fibers, (b) PCL based fibers with the addition of HAP, (c) PCL based fibers with the addition of HAP and 5 wt% of AMX, (d) PCL based fibers with the addition of HAP and 7 wt% of AMX.

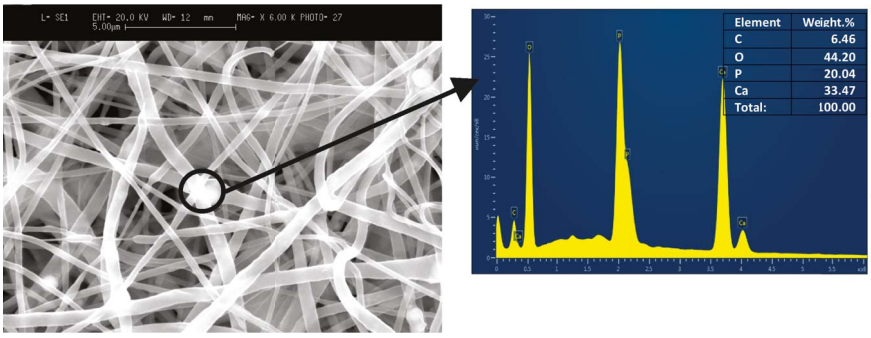

Figure 5. EDX analysis of biologically soluble *PCL/HAP/AMX* based scaffold.

plates with *S. aureus* bacterial culture, the growth inhibition zone after 24 h was 3.8 mm ± 0.07. After 72 h, it did not increase in diameter and still was 3.8 mm ± 0.14, with no signs of secondary contamination. The growth of inhibition zone in the plates with the bacterial culture of *E. faecalis* was 4.5 mm ± 0.04 and 5.3 mm ± 0.14 after 24 and 72 h, respectively. Over time, an increase in the inhibition zone growth indicated a prolonged antimicrobial effect of the synthesized bioscaffold on the specified types of pathogen. It was found that AMX incorporated into the structure of the bioscaffold affects gram-positive cocci *S. aureus* and *E. faecalis*. Moreover, as far as *E. faecalis* is concerned, a prolonged antimicrobial effect is noted. The process of electrospinning during the synthesis of bioscaffolds and the presence of HAP in its structure does not affect the antimicrobial properties of the obtained material. As expected,

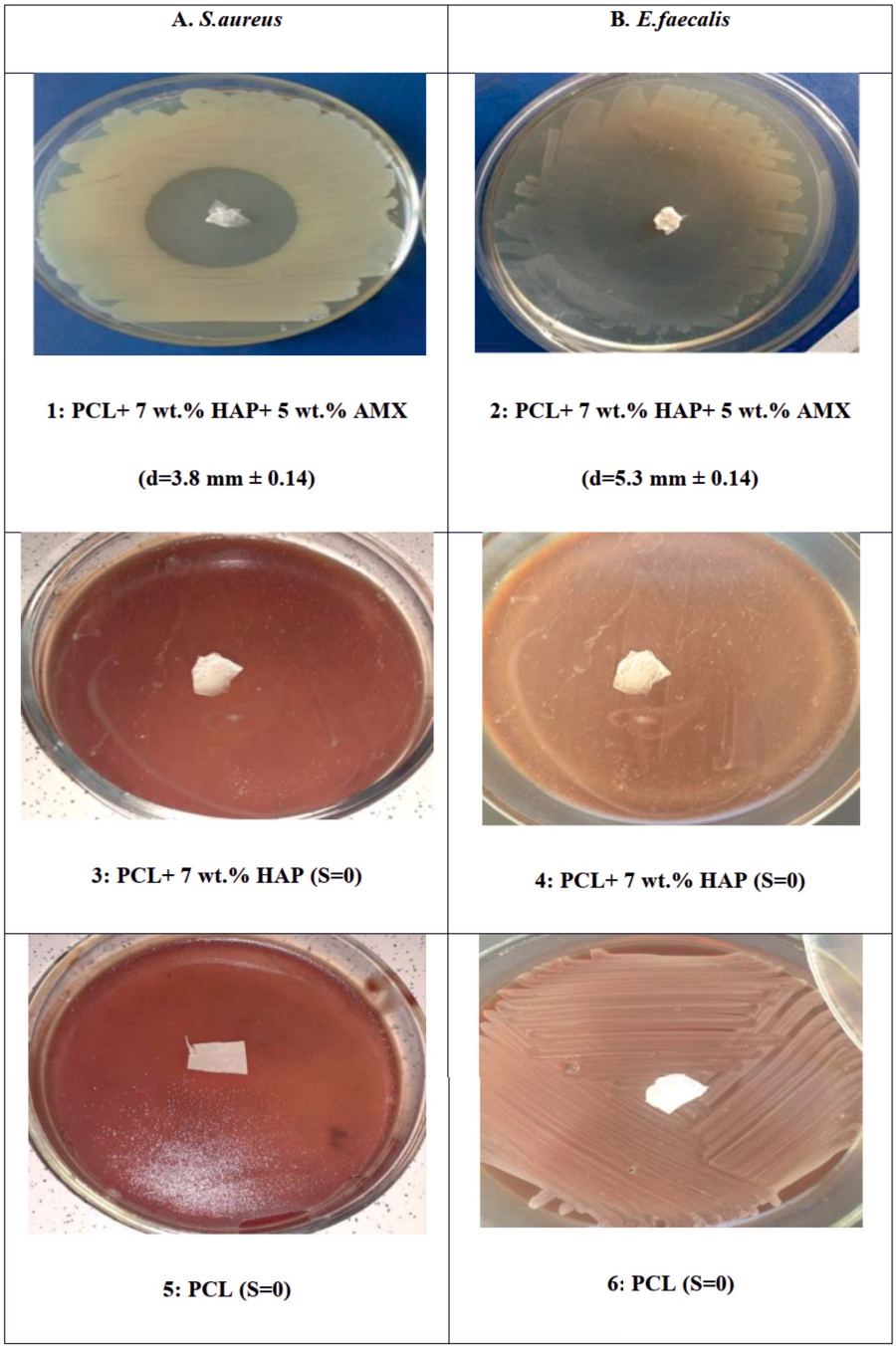

Figure 6. Inhibition of (a) *S. aureus* and (b) *E. faecalis* growth at day 3 by PCL/HAP/AMX based scaffolds (PCL + 7 wt% HAP + 5 wt% AMX). PCL + 7 wt% HAP (3,4) and pure PCL (5,6) used as a negative controls.

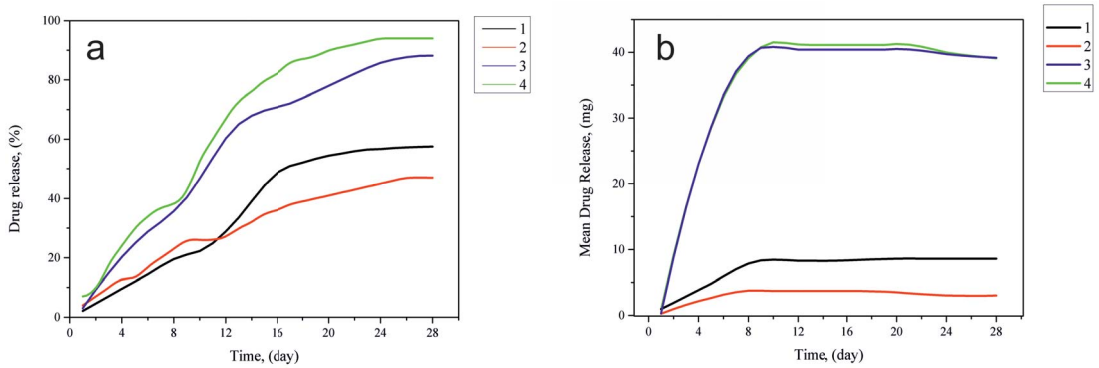

Figure 7. Kinetics of AMX release in (a) percentage and (b) quantitative terms from the obtained PCL/HAP/AMX based scaffolds: (1) PCL/AMX (diameter of fibers 300 nm); (2) PCL/HAP/AMX (diameter of fibers 300 nm); (3) PCL/AMX (diameter of fibers 100 nm); (4) PCL/HAP/AMX (diameter of fibers 100 nm).

there was no growth of the inhibition zone in control groups (pure PCL and PCL + 7 wt% HAP) after the observation time, regarding both studied pathogens. Thus, we show the growth inhibition at day 3 of *S. aureus* and *E. faecalis*, the prominent representatives of root canals microflora, by antibiotic-containing electrospun scaffold (PCL + 7 wt% HAP+ 5 wt% AMX). Two types of samples (PCL + 7 wt% HAP) and pure PCL were used as a negative control. Thereby significant differences between the indicators of the antimicrobial action of the specified samples were revealed (Figure 6).

The kinetics of AMX release from the obtained scaffolds was observed during a 4-week period. The resulting drug release curves are shown in Figure 7.

The antibiotic release from the scaffolds without the addition of HAP (Figure 7a) was 25 mg and increased to 42 mg at the end of the observation period. The cumulative percentage of AMX release amounted to about 94% of the total weight of the antibiotic. These observations show that in the case of scaffolds with a thickness of 0.15 mm, the antibiotic is mostly located on the surface of polymer fibers, ensuring its complete release. It is found that when increasing the fiber diameter from 100 nm to 300 nm, the total antibiotic release was 75% over a 4-week observation period (Figure 7c). This is due to the fact that a change in the diameter of the fibers allows the drug to penetrate deep into the scaffold. The presence of HAP in the scaffold structure has practically no effect on the release of the antibiotic. The studies have shown that the kinetics of drug release depends on the diameter of polymer fibers, their surface morphology, and the drug distribution throughout the scaffold's structure.

4. Conclusion

The studies on the preparation of composite biologically soluble scaffolds from synthesized HAP and an antibiotic (AMX) have shown their promising use for local drug delivery in endodontic treatment. It was found that the HAP powder, obtained by chemical deposition from an aqueous solution of orthophosphoric acid, has a purity of 97% and particle size of up to 2 μm. The post-thermal treatment of HAP at a temperature of 1100 °C in an air medium for 2 h allows obtaining HAP with physicochemical properties close to those of the inorganic component of human bone with enhanced crystallinity. The cumulative percent release from composite biologically soluble scaffolds was stated as about 94% of the total antibiotic weight over 4 weeks. An increase in the fiber diameter from 100 nm to 300 nm results in the decrease of the total release of the antibiotic from 98% to 75% during a 4-week observation period. As a result of the standard diffusion test in agar, significant inhibition of the studied bacterial strains growth was revealed when exposed to a scaffold sample based on polymer fibers containing AMX and HAP. In the plates with the bacterial culture of *S. aureus*, the growth of the inhibition zone after 18 h reached 3.8 ± 0.07 mm, and after 72 h—3.8 ± 0.14 mm. The inhibition zone growth in the plates with the bacterial culture of

E. faecalis was 4.5 ± 0.04 mm after 18 h and 5.3 ± 0.14 mm after 72 h. Thus, the obtained results confirm the efficiency of electrospinning for obtaining biologically soluble scaffolds for endodontic therapy. Moreover, the change in HAP concentrations and drug in the resulting scaffolds makes them promising candidates for biologically soluble scaffolds and other areas such as drug delivery and bone substitute implants.

Supplementary data

Supporting information for this article is available on the journal's website under https://doi.org/10.5802/crchim.58 or from the author.

References

[1] B. Michot, S. M. Casey, J. L. Gibbs, *J. Endod.*, 2020, **46**, 950-956.

[2] S. S. Mirsasaani, M. Hemati, E. S. Dehkord, G. T. Yazdi, D. A. Poshtiri, "Nanotechnology and nanobiomaterials in dentistry", in *Nanobiomaterials in Clinical Dentistry*, Elsevier, 2019, 19-37.

[3] S. Navarro-Suarez, A. Flores-Palma, R. Flores-Ruiz, J.-L. Gutiérrez-Pérez, D. Torres-Lagares, "Nanobiomaterials in dentistry", in *Nanobiomaterials*, Elsevier, 2018, 297-318.

[4] Y. Chen, X. Li, J. Wu, W. Lu, W. Xu, B. Wu, *J. Dent. Sci.*, 2020, **16**, no. 1, 318-326.

[5] A. Daghrery, Z. Aytac, N. Dubey, L. Mei, A. Schwendeman, M. C. Bottino, *Colloid. Surface. B*, 2020, **191**, article no. 111011.

[6] S. Vaseenon, N. Chattipakorn, S. C. Chattipakorn, *Arch. Oral Biol.*, 2020, **109**, article no. 104574.

[7] B. Dzeletovic, N. Aleksic, D. Radak, D. Stratimirovic, L. Djukic, D. Stojic, *J. Endod.*, 2020, **46**, 358-363.

[8] R. Cameron, E. Claudia, W. Ping, S. Erin, N. B. Ruparel, *J. Endod.*, 2019, **45**, 1119-1125.

[9] K. Ruksakiet, L. Hanák, N. Farkas, P. Hegyi, W. Sadaeng, L. M. Czumbel, T. Sang-ngoen, A. Garami, A. Mikó, G. Varga, Z. Lohinai, *J. Endod.*, 2020, **46**, 1032-1041.

[10] W. Ye, L. Yeghiasarian, C. W. Cutler, B. E. Bergeron, S. Sidow, H. H. K. Xu, L. Niu, J. Ma, F. R. Tay, *J. Dent.*, 2019, **91**, article no. 103231.

[11] C. Zeng, M. M. Meghil, M. Miller, Y. Gou, C. W. Cutler, B. E. Bergeron, L. Niu, J. Ma, F. R. Tay, *J. Dent.*, 2018, **72**, 71-75.

[12] I. R. Bordea, R. Hanna, N. Chiniforush, E. Grădinaru, R. S. Câmpian, A. Sîrbu, A. Amaroli, S. Benedicenti, *Photodiag. Photodyn. Ther.*, 2020, **29**, article no. 101611.

[13] E. AlShwaimi, D. Bogari, R. Ajaj, S. Al-Shahrani, K. Almas, A. Majeed, *J. Endod.*, 2016, **42**, 1588-1597.

[14] F. R. Sultanov, C. Daulbayev, B. Bakbolat, Z. A. Mansurov, *Eurasian Chem. Tech. J.*, 2018, **20**, 195.

[15] A. Karczewski, S. A. Feitosa, E. I. Hamer, D. Pankajakshan, R. L. Gregory, K. J. Spolnik, M. C. Bottino, *J. Endod.*, 2018, **44**, 155-162.

[16] H. Urena-Saborio, G. Rodríguez, S. Madrigal-Carballo, S. Gunasekaran, *Materialia*, 2020, **11**, article no. 100687.

[17] X. Yu, T. Wang, W. Yin, Y. Zhang, *Int. J. Hydrog. Energ.*, 2019, **44**, 2704-2710.

[18] M. C. Bottino, D. Pankajakshan, J. E. Nör, *Dent. Clin. N. Am.*, 2017, **61**, 689-711.

[19] A. B. Paula, M. Laranjo, C.-M. Marto, S. Paulo, A. M. Abrantes, J. Casalta-Lopes, M. Marques-Ferreira, M. F. Botelho, E. Carrilho, *J. Evid. Based Dent. Pr.*, 2018, **18**, 298-314.

[20] W. Zhang, Y. Zheng, H. Liu, X. Zhu, Y. Gu, Y. Lan, J. Tan, H. Xu, R. Guo, *Mater. Sci. Eng.*, 2019, **103**, article no. 109736.

[21] Y.-C. Chiang, H.-H. Chang, C.-C. Wong, Y.-P. Wang, Y.-L. Wang, W.-H. Huang, C.-P. Lin, *Dent. Mater.*, 2016, **32**, 1197-1208.

[22] B. Alliot-Licht, A. Jean, M. Gregoire, *Arch. Oral Biol.*, 1994, **39**, 481-489.

[23] C. Daulbayev, Z. Mansurov, G. Mitchell, A. Zakhidov, *Euras. Chem. Tech. J.*, 2018, **20**, 119.

[24] R. K. Sübay, S. Aşci, *Oral Surg. Oral Med. Oral Pathol.*, 1993, **76**, 485-492.

[25] F. Sultanov, C. Daulbayev, B. Bakbolat, O. Daulbayev, M. Bigaj, Z. Mansurov, K. Kuterbekov, K. Bekmyrza, *Chem. Phys. Lett.*, 2019, **737**, article no. 136821.

[26] C. B. Daulbaev, T. P. Dmitriev, F. R. Sultanov, Z. A. Mansurov, E. T. Aliev, *J. Eng. Phys. Thermophy.*, 2017, **90**, 1115-1118.

[27] H. Rodríguez-Tobías, G. Morales, D. Grande, *Mater. Sci. Eng.*, 2019, **101**, 306-322.

[28] S. Mohandesnezhad, Y. Pilehvar-Soltanahmadi, E. Alizadeh, A. Goodarzi, S. Davaran, M. Khatamian, N. Zarghami, M. Samiei, M. Aghazadeh, A. Akbarzadeh, *Mater. Chem. Phys.*, 2020, article no. 123152.

[29] F. R. Sultanov, C. Daulbayev, B. Bakbolat, Z. A. Mansurov, A. A. Urazgaliyeva, R. Ebrahim, S. S. Pei, K.-P. Huang, *Carbon Lett.*, 2020, **30**, 81-92.

[30] A. Hrioua, A. Loudiki, A. Farahi, M. Bakasse, S. Lahrich, S. Saqrane, M. A. El Mhammedi, *Bioelectrochemistry*, 2021, **137**, article no. 107687.

[31] N. Kourkoumelis, I. Balatsoukas, M. Tzaphlidou, *J. Biol. Phys.*, 2012, **38**, 279-291.

[32] E. Loughrill, D. Wray, T. Christides, N. Zand, *Matern. Child Nutr.*, 2017, **13**, article no. e12368.

[33] Y. Ma, A. Wang, J. Li, Q. li, Q. Han, Y. Chen, S. Wang, X. Zheng, H. Cao, S. Bai, *Colloid. Surface. A*, 2020, **596**, article no. 124740.

[34] T. V. Safronova, I. I. Selezneva, S. A. Tikhonova, A. S. Kiselev, G. A. Davydova, T. B. Shatalova, D. S. Larionov, J. V. Rau, *Bioact. Mater.*, 2020, **5**, 423-427.

[35] M. Rahmati, D. K. Mills, A. M. Urbanska, M. R. Saeb, J. R. Venugopal, S. Ramakrishna, M. Mozafari, *Prog. Mater. Sci.*, 2020, article no. 100721.

[36] A. Vahdat, B. Ghasemi, M. Yousefpour, *S. Afr. J. Chem. Eng.*, 2020, **33**, 90-94.